

Skin-Friction and Forced Convection from an Isothermal Rough Plate

Aubrey G. Jaffer
e-mail: agj@alum.mit.edu

Abstract

A novel analysis of the turbulence generated by steady flow along a self-similar roughness yields new formulas for skin-friction coefficient and forced convection, both of which apply to both self-similar and self-dissimilar isothermal plates having isotropic root-mean-squared (RMS) height-of-roughness $\varepsilon > 0$:

$$f_c = \frac{1}{3 \ln^2(L/\varepsilon)} \quad \text{Nu} = \frac{\text{Re Pr}^{1/3}}{6 \ln^2(L/\varepsilon)} \quad \frac{L}{\varepsilon} \gg 1$$

When corrected for a scaling problem in the sand-roughness metric, the total skin-friction coefficient formulas from both Prandtl and Schlichting and Mills and Hang are in agreement with the new formula in “the completely rough regime” (large Reynolds numbers).

This new theory differs from Prandtl and Schlichting in the “transitional rough regime”. Where their theory predicted a 10% dip in skin-friction coefficient specifically for sand-roughened plates, the new theory predicts zero dependence on Reynolds number for isotropic roughness generally. Measurements of self-dissimilar plates by the author and by Pimenta, Moffat, and Kays support this new theory in both the transitional rough and completely rough regimes.

Keywords: turbulence; skin-friction; profile roughness; sand-roughness; forced-convection

Table of Contents

| | |
|--|----|
| <i>Introduction</i> | 2 |
| <i>Prior Work</i> | 3 |
| <i>Roughness</i> | 4 |
| <i>Self-Similar Profile Roughness</i> | 5 |
| <i>Self-Similar Surface Roughness</i> | 6 |
| <i>Vertical Roughness Travel</i> | 7 |
| <i>Skin-Friction and Forced Convection</i> | 8 |
| <i>Self-Dissimilar Roughness</i> | 8 |
| <i>Physical Measurements</i> | 9 |
| <i>Sand-Roughness</i> | 10 |
| <i>Transitional Rough Regime</i> | 12 |
| <i>Roughness in Pipes</i> | 13 |
| <i>Conclusions</i> | 14 |
| <i>Nomenclature</i> | 14 |
| <i>References</i> | 15 |

1. Introduction

The skin-friction drag¹ of a rough surface is important to the fluid dynamics of vehicles and turbines. The related phenomenon of forced convection (from a rough surface) has application to modeling weather and the thermal behavior of buildings.

Forced flow along a flat plate with a rough surface is different in character from forced flow along a smooth surface because the peaks of roughness protrude through what would otherwise be a laminar boundary-layer adjacent to the plate.

Prandtl and Schlichting[1] assert that the plate's height-of-roughness decreases relative to the depth of the boundary-layer growing along the plate in the direction of flow. This would not be true of a surface with self-similar roughness (as defined in Section 3). The ratio of the height-of-roughness to the characteristic-length of the plate being constant means that the height-of-roughness grows linearly with plate length (from its leading edge). The combination of boundary-layer disruption near the leading edge with linear growth of the height-of-roughness results in the whole surface shedding rough turbulence.

Prandtl and Schlichting split their analysis into three parts based on boundary-layer depth. For the present work, self-similarity requires only a single analysis. Moreover, this single analysis does not employ boundary-layer theory.

Turbulent flow can occur adjacent to plates in an isobaric environment; but turbulent flow in pipes and ducts is not isobaric.² Prandtl and Schlichting applied the analysis of rough pipe flow to rough plates; the present work does not, although conversions between height-of-roughness metrics appear to work the same for pipes and plates.

Section 2 describes prior work and demonstrates a scaling problem with the legacy "sand-roughness" metric.

Section 3 defines profile and surface roughness, the root-mean-squared (RMS) height-of-roughness metric, and a type of self-similarity for profile roughness functions.

Section 4 gives three examples of discrete self-similar profile roughness functions.

Section 5 shows the surfaces generated by summing each discrete profile function with itself rotated 90°.

Section 6 derives a single formula for the total vertical travel of a conforming flow for two of the discrete profile roughness functions from Section 4. The ratio of vertical roughness travel to horizontal travel is used to scale the bulk fluid velocity to the "roughness velocity".

Section 7 formulates the skin-friction coefficient as the square of the ratio of roughness velocity to bulk fluid velocity.

Section 8 considers the new theory's application to rough surfaces which lack self-similarity (thus are "self-dissimilar").

Section 9 compares the new forced convection formula with convection measurements of a bi-level, self-dissimilar plate.

Section 10 examines the sand-roughness metric and its relation to the RMS height-of-roughness metric, enabling comparisons with prior works, which are presented. The close match to Mills and Hang[2] (based on measurements from Pimenta, Moffat, and Kays[3]) supports the new theory in the fully rough regime.

Section 11 discusses the behavior of rough plates at low Reynolds numbers (Re), the transitional rough regime. The present work's prediction of constant skin-friction coefficient is supported by measurements of the bi-level (self-dissimilar) plate and measurements by Pimenta, Moffat, and Kays[3] of their sphere-roughened plate.

Section 12 speculates on the implications of this work to roughness in pipes (and ducts).

¹ Skin-friction drag is the pressure opposing the flow due to viscous dissipation of the turbulence generated by flow along the surface.

² Skin-friction drag causes pressure loss in flow through the pipe.

2. Prior Work

In 1934 Prandtl and Schlichting published *Das Widerstandsgesetz rauher Platten (The Resistance Law for Rough Plates)*[1], which brilliantly infers a relation for skin-friction resistance for rough plates from their analysis of Nikuradse’s measurements of sand glued inside pipes (“sand-roughness”). In *Boundary-layer theory*[4] Prandtl and Schlichting give a formula for fully rough (large Re) total skin-friction coefficient for a rough flat plate in terms of its sand-roughness k_S and the characteristic-length L of the plate in the direction of flow:

$$c_f = \left(1.89 + 1.62 \log_{10} \frac{L}{k_S}\right)^{-2.5} \quad 10^2 < \frac{L}{k_S} < 10^6 \quad (1)$$

In *On the Skin Friction Coefficient for a Fully Rough Flat Plate*[2], Mills and Hang present a formula which they claim to be more accurate than the Prandtl-Schlichting formula (1) on the local skin-friction coefficient measurements from Pimenta, Moffat, and Kays[3]. Their corrected³ total skin-friction coefficient formula is:

$$C_D = \left(2.035 + 0.618 \ln \frac{L}{k_S}\right)^{-2.57} \quad 750 < \frac{L}{k_S} < 2750 \quad (2)$$

In *Viscous Fluid Flow*[5], White gives a formula for fully rough local (not total) skin-friction coefficient:

$$C_f = \left(1.4 + 3.7 \log_{10} \frac{x}{k_S}\right)^{-2} \quad \frac{x}{k_S} > \frac{\text{Re}_x}{1000} \Rightarrow \frac{L}{k_S} > \frac{\text{Re}}{1000} \quad (3)$$

Numerical integration of the local skin-friction coefficient formula from Prandtl and Schlichting gives results close to their total formula (1) when the lower limit of integration is $L/k_S \approx 0.188$. Numerical integration of the local formula from Mills and Hang is less successful and is very sensitive to the lower limit of integration. Numerical integration of formula (3) is also sensitive, but adjusting the lower bound does not produce a curve with slope close to the others. White doesn’t give guidance on this issue or compare the formula to experiment; it is not pursued further here.

The roughness in these works is reported in Nikuradse’s sand-roughness metric k_S , the height of “coarse and tightly placed roughness elements such as for example coarse sand grains glued on the surface”. Prandtl and Schlichting[1] gives the parameters of Nikuradse’s sand coatings, which are reproduced in the left two columns of Table 1.

| k_S | grains/cm ² | k_S^{-2} |
|--------|------------------------|------------------------|
| .08 cm | 150 | 156.25/cm ² |
| .04 cm | 590 | 625/cm ² |
| .02 cm | 1130 | 2500/cm ² |
| .01 cm | 4600 | 10000/cm ² |

Table 1 Nikuradse’s sand coatings

Because their packing densities scale as the inverse of grain diameter squared, the .08 cm and .04 cm sand coatings should scale correctly as long as the glue thickness is proportional to grain diameter. Similarly the .02 cm and .01 cm sand coatings should scale.

The two coarsest coatings (largest k_S values) had packing densities slightly less than a square packing. The other two had packing densities less than half that of a square packing. But comparing the .02 cm and .04 cm sand coatings, their packing density ratio is nearly 1:2, not 1:4. Thus formulas (1) and (2) will have incorporated a scale error (between measurements of large and small k_S) and should not be trusted for L/k_S values much larger than 1000 (507 is the largest rough pipe L/k_S value in Schlichting[4] Fig. 20.18).

Section 10 compares formulas (1) and (2) with the present work.

³ The Mills and Hang[2] published formula had a “6” where a “0” should have been in the first constant:

$$C_D = \left(2.635 + 0.618 \ln \frac{L}{k_S}\right)^{-2.57}$$

All of their measurement comparisons were of local skin-friction coefficient, which used a different formula. Figure 10 shows traces for both the corrected and uncorrected total formulas.

3. Roughness

Let profile roughness be a function $z(x)$ where $0 \leq x \leq L$ is distance from the leading edge in the direction of flow.

Let surface roughness be a function $z(x, y)$ of the x and y coordinates in the surface of the plate. Functions being single-valued, there are no tunnels or overhangs.

Although vortexes can arise in two-dimensional systems, turbulence is a three-dimensional phenomena. The random velocity fluctuations must be isotropic at all but the coarsest length scales. In order that the random fluid velocities resulting from interaction with the plate roughness are not skewed, $z(x, y)$ should be roughly isotropic; rotating x and y should not materially affect the behavior of the system. A surface composed of parallel ridges and valleys would not meet this criterion.

This also applies to profile roughness. A parcel of fluid will scatter off its first encounter with roughness; its resulting direction will likely not be parallel to the bulk flow. So the roughness perpendicular to the flow figures in the behavior of profile roughness. The simplest roughly isotropic treatment is $z(x, y) = z(x) + z(y)$.

Consider the roughness profile $z(x)$. Its mean height \bar{z} and root-mean-squared height-of-roughness ϵ are:

$$\bar{z} = \frac{1}{L} \int_0^L z(x) dx \quad \epsilon = \sqrt{\frac{1}{L} \int_0^L [z(x) - \bar{z}]^2 dx} \quad (4)$$

For a surface roughness $z(x, y)$ the mean height \bar{z} and root-mean-squared height-of-roughness ϵ are:

$$\bar{z} = \frac{1}{L^2} \int_0^L \int_0^L z(x, y) dx dy \quad \epsilon = \sqrt{\frac{1}{L^2} \int_0^L \int_0^L [z(x, y) - \bar{z}]^2 dx dy} \quad (5)$$

The roughness functions $z(x)$ and $z(x, y)$ need not be continuous to be integrable. Local flow properties may not be well-defined anywhere. The present analysis is of total skin-friction coefficient only.

A profile roughness function $z(x)$ has self-similar roughness with (integer) branching factor $n \geq 2$ if the RMS height-of-roughness of $z(x)$ over an interval $x_0 < x < x_n$ is n times the RMS height-of-roughness of $z(x)$ over each (evenly divided) sub-interval $x_j < x < x_{j+1}$ for $0 \leq j < n$ at a succession of scales converging to 0.⁴ A consequence of this definition of self-similar roughness is that the ratio of the length of the interval $L = x_n - x_0$ to its RMS height-of-roughness ϵ will be invariant over its succession of scales converging to 0.

Self-similarity is of interest because the skin-friction coefficient f_c , which will be formulated in Section 7, is a function of L/ϵ . If the roughness is self-similar, then L/ϵ and $f_c(L/\epsilon)$ will be constant over the span of the roughness profile.

In the three examples of self-similar profile roughness in Section 4, the roughness function is simply a permutation of the linear ramp $z(x) = x$ from $x = 0$ to $x = w$. Because the RMS height-of-roughness calculation depends only on the z values and not their relation to x , for all ramp-permutation profile roughness:

$$\epsilon = \sqrt{\frac{1}{w} \int_0^w [x - w/2]^2 dx} = \frac{w}{\sqrt{12}} \quad (6)$$

This raises the question of whether a linear ramp, which is the identity permutation of a linear ramp, can produce fully rough turbulence from a steady flow. A ramp doesn't meet the isotropy requirement because $z(x, y) = x + y$ has zero profile roughness parallel to $x = -y$. A linear ramp being disqualified, are self-similar roughness profiles possible? Section 4 constructs three examples of self-similar roughness profiles.

⁴ Note that $z(x_j)$ values contribute to the interval height-of-roughness, but not to any sub-interval height-of-roughness.

4. Self-Similar Profile Roughness

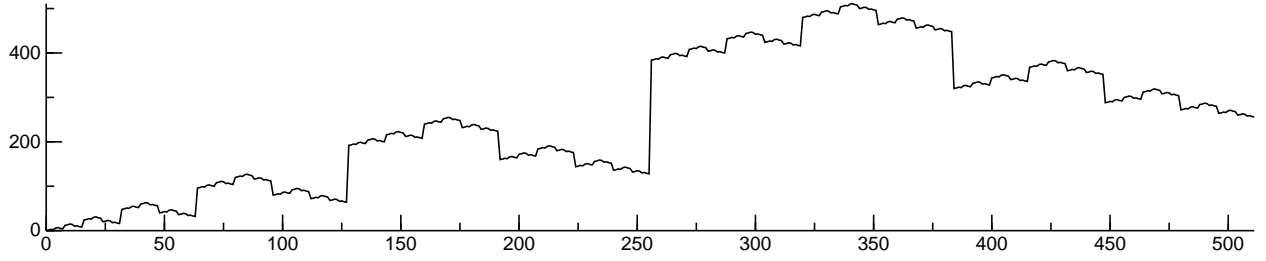


Figure 1 Gray-code profile roughness

The integer Gray-code sequence $G(x, w)$ with $0 \leq x < w = 2^j$ shown in Figure 1 has an RMS height-of-roughness $\epsilon = w/\sqrt{12}$ from equation (6) and is a self-similar roughness (when bisected) as seen by its recurrence:

$$G(x, w) = \begin{cases} x, & \text{if } w = 1; \\ w + G(w - 1 - (x \bmod w), w/2), & \text{if } \lfloor x/w \rfloor = 1; \\ G(x \bmod w, w/2), & \text{otherwise.} \end{cases} \quad (7)$$

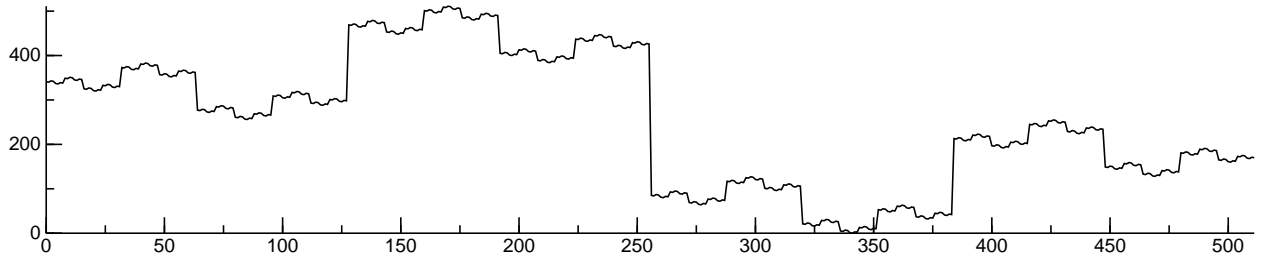


Figure 2 Wiggliest self-similar profile roughness

The integer sequence $W(x, w)$ which reverses at each bifurcation produces the wiggliest possible self-similar roughness with $0 \leq x < w = 2^j$ and is shown in Figure 2; it has an RMS height-of-roughness $\epsilon = w/\sqrt{12}$:

$$W(x, w) = \begin{cases} x, & \text{if } w = 1; \\ \lfloor x/w \rfloor w + W(w - 1 - (x \bmod w), w/2), & \text{otherwise.} \end{cases} \quad (8)$$

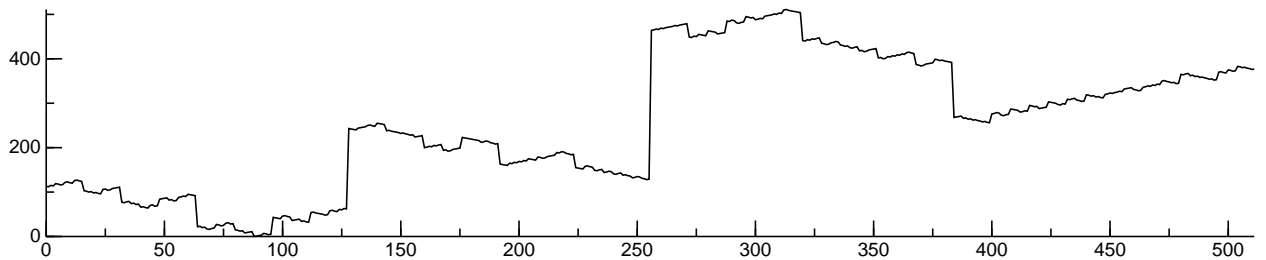


Figure 3 Randomly reversing bifurcation profile roughness

Figure 3 shows an integer sequence generated by recursive-descent with random reversing at each bifurcation. It has an RMS height-of-roughness $\epsilon = w/\sqrt{12}$; its roughness is approximately self-similar.

5. Self-Similar Surface Roughness

An $L \times L$ self-similar roughness function $z(x, y)$ can be constructed from a profile roughness function $z(x) = Y(xw/L, w)/w$:

$$z(x, y) = z(x) + z(y) = \frac{1}{w} \left[Y\left(x \frac{w}{L}, w\right) + Y\left(y \frac{w}{L}, w\right) \right] \quad w = 2^j$$

When the profile roughness is a linear ramp permutation, the surface height-of-roughness ε is $\sqrt{2}$ times the profile height-of-roughness ϵ .

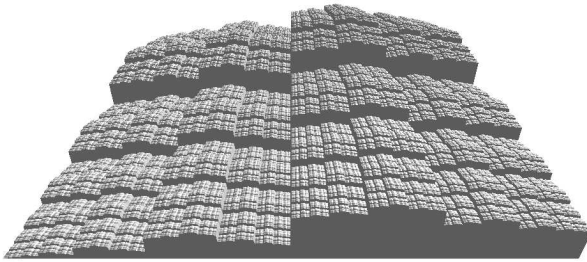


Figure 4 Gray-code surface roughness

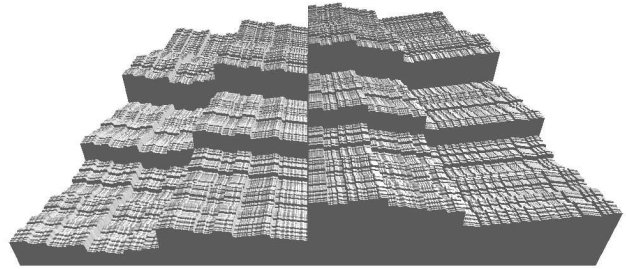


Figure 5 Random reversing surface roughness

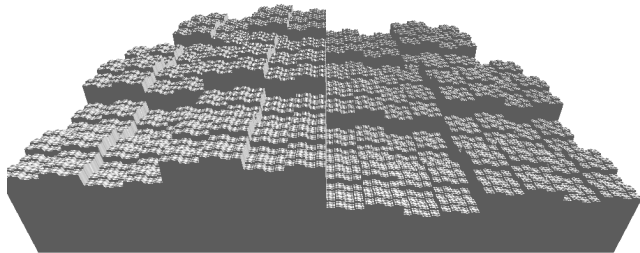


Figure 6 Wiggliest self-similar roughness

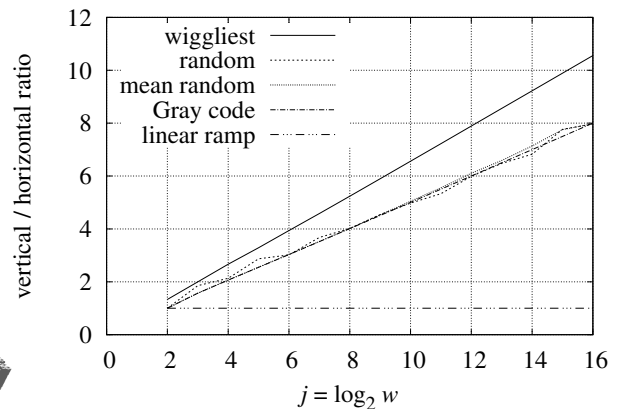


Figure 7 Travel along profile roughness

Figures 4 and 5 show squared Gray-code and random-reversal roughness corresponding to Figures 1 and 3 respectively. These look somewhat like faulted and weathered granite outcroppings.

Figure 6 shows squared wiggly roughness corresponding to Figure 2. Unnatural in appearance, it resembles tire treads.

6. Vertical Roughness Travel

In order to convert some of the flow to rough turbulence, parcels of fluid must move in directions not parallel to the bulk flow. Such movement could result from deflection of flow by the vertical spans of discrete profile roughness; the amount of turbulence produced would grow with the height-of-roughness.

For roughness profile $Y(x, w)$, the sum of the lengths of all horizontal segments is $w - 1 = 2^j - 1$. The sum of the absolute value of the length of each vertical segment is:

$$\sum_{x=0}^{2^j-2} |Y(x, 2^j) - Y(x+1, 2^j)| \quad (9)$$

If a parcel of fluid were to trace a roughness profile $Y(x, w)$ from $x = 0$ to $x = w - 1$, then $w - 1$ is the horizontal distance it would travel, while formula (9) is the vertical distance.

Shown in Figure 7 is the vertical to horizontal travel ratio versus j , the base-2 logarithm of w . The slope is 1/2 for the Gray-code and random-reversal cases, but 2/3 for the wiggliest roughness W . And the vertical segments in Figure 2 are indeed longer than the vertical segments in Figures 1 and 3.

A wiggliest roughness profile $W(x, w)$ is an extreme case; it reverses vertical direction at each increment of x . For each wiggliest roughness profile there are many more random bifurcation roughness profiles. Going forward, $W(x, w)$ will be excluded as an outlier.

From Figure 7 the vertical to horizontal travel ratio for the Gray-code and random-reversal sequences is close to:

$$\frac{j}{2} = \frac{\log_2 w}{2} \quad (10)$$

Formula (10) is unbounded as w increases. At some scale of w , vertical fluid movement by a distance of L/w will induce negligible turbulence. The argument to \log_2 must be dimensionless. $\log_2(\epsilon/L)$ is always negative because $\epsilon \ll L$; $\log_2(L/\epsilon)$ is positive, but inverts the sense of formula (10). Letting $w = L/\epsilon$, the ratio of vertical to horizontal travel is then:

$$\frac{2}{\log_2(L/\epsilon)} \quad (11)$$

The maximum peak-to-valley height is $\sqrt{12}$ times the RMS height-of-roughness ϵ . So the vertical to horizontal ratio should be scaled:

$$\frac{1}{\sqrt{12}} \frac{2}{\log_2(L/\epsilon)} = \frac{1}{\sqrt{3} \log_2(L/\epsilon)} \quad (12)$$

In *Self-Similar Processes Follow a Power Law in Discrete Logarithmic Space*[6] Newberry and Savage demonstrate that some self-similar systems which are modeled using continuous power-law probability distributions (such as the Pareto distribution) are better modeled using discrete power-law distributions.

The present work uses their idea in reverse. Conversion of flow into turbulence by contact with discrete self-similar roughness having been modeled above, the turbulence generation by a continuous self-similar roughness will be inferred using a random variable.

The base-2 logarithm is an artifact of the discrete roughness functions from Section 4. The analogous mean field theory is to treat $Z = |\Delta Y|$ as a continuous random variable having a Pareto distribution where the frequency of Z is inversely proportional to Z^2 :

$$1 \Big/ \left[\int_{\epsilon}^L \frac{\sqrt{3} Z}{Z^2} dZ \right] = \frac{1}{\sqrt{3} \ln(L/\epsilon)} \quad (13)$$

Note that the surface height-of-roughness ϵ is used in equation (13) instead of the profile height-of-roughness ϵ in equation (12).

7. Skin-Friction and Forced Convection

For a rough flat surface subjected to a steady flow parallel to its surface which is sufficiently fast to generate turbulence, the skin-friction drag is the pressure opposing the flow due to viscous dissipation of that turbulence.⁵

The skin-friction coefficient f_c is the ratio of the shear stress τ , which is primarily the skin-friction drag when $L/\varepsilon \gg 1$, to the flow's kinetic energy density $\rho u^2/2$.

$$f_c = \frac{\tau}{\rho u^2/2} \quad (14)$$

f_c is dimensionless; both τ and $\rho u^2/2$ have units of pressure, $\text{kg}/(\text{m} \cdot \text{s}^2)$.

Scaling by the vertical to horizontal travel ratio from formula (13) converts a horizontal velocity u to a vertical roughness velocity u_R , from which τ is derived:

$$u_R = \frac{u}{\sqrt{3} \ln(L/\varepsilon)} \quad \tau = \frac{\rho u_R^2}{2} = \frac{\rho u^2}{6 \ln^2(L/\varepsilon)} \quad \frac{L}{\varepsilon} \gg 1 \quad (15)$$

Combining equations (15) and (14) produces a formula for f_c dependent only on L/ε :

$$f_c = \frac{1}{3 \ln^2(L/\varepsilon)} \quad \frac{L}{\varepsilon} \gg 1 \quad (16)$$

Figure 10 plots f_c over four decades of L/ε .

The Chilton and Colburn J-factor analogy (17) relates friction factors to turbulent forced convective heat transfer.

$$\text{Nu} = \frac{f_c}{2} \text{Re Pr}^{1/3} \quad (17)$$

Combining equation (17) with equation (16) produces a formula for forced convection:

$$\text{Nu} = \frac{\text{Re Pr}^{1/3}}{6 \ln^2(L/\varepsilon)} \quad \frac{L}{\varepsilon} \gg 1 \quad (18)$$

8. Self-Dissimilar Roughness

What can be learned from physical measurements of skin-friction or forced-convection from rough plates?

If a plate with a discrete self-similar roughness profile were measured and had the predicted dependence on Re , it could confirm the new formulas for a very limited class of roughness. If a plate with a continuous self-similar roughness were tested, then the class would be larger, but still restricted to self-similarity. If measurements (over a range of Re values) of multiple self-dissimilar plates with isotropic roughness were found to conform to the new formulas, then that would be compelling evidence that the new formulas reflect a physical law of turbulent flow along isotropic surface roughness.

The rough surface tested by Pimenta, Moffat, and Kays[3] was composed of 11 sheets of densely packed metal balls 1.5 mm in diameter “arranged such that the surface has a regular array of hemispherical roughness elements.” Such a surface should behave similarly to a sand-roughened plate, but with an RMS height-of-roughness which can be calculated. Being repeating patterns, both sphere-roughened and sand-roughened surfaces are self-dissimilar.⁶

The results of testing self-dissimilar plates are presented in Sections 9, 10, and 11.

⁵ As the height of roughness ε grows relative to the characteristic-length L , pressure drag (which is not dissipative) grows. $L/\varepsilon \gg 1$ constrains the system so that skin-friction drag dominates pressure drag.

⁶ Self-similarity is similarity between shapes at different scales; but these spheres are the same size.

9. Physical Measurements

The Convection Machine[7] bi-level plate surface was composed of (676) $8.28 \text{ mm} \times 8.28 \text{ mm} \times 6 \text{ mm}$ posts spaced on 11.7 mm centers. The area of the top of each post was 0.686 cm^2 , half of its 1.37 cm^2 cell. The root-mean-squared height-of-roughness was 3 mm. The equal-area bi-level architecture provides the largest RMS height-of-roughness possible in a 6 mm peak-to-valley span. And this surface has no self-similarity.⁷

Applying formula (18) yields $\text{Nu} = 0.0078 \text{ Re Pr}^{1/3}$. The corresponding trace “rough turbulent asymptote” in Figure 8 matches the “ $\Delta T = 11 \text{ K}$ measured” convection within $\pm 3\%$ from $\text{Re} = 5500$ to 50000 .⁸

The self-dissimilar bi-level plate behaving compatibly with formula (18) derived from self-similar analysis supports the claim that formulas (16) and (18) are intrinsic to turbulent flow along isotropic roughness and not specific to self-similar roughness profiles.

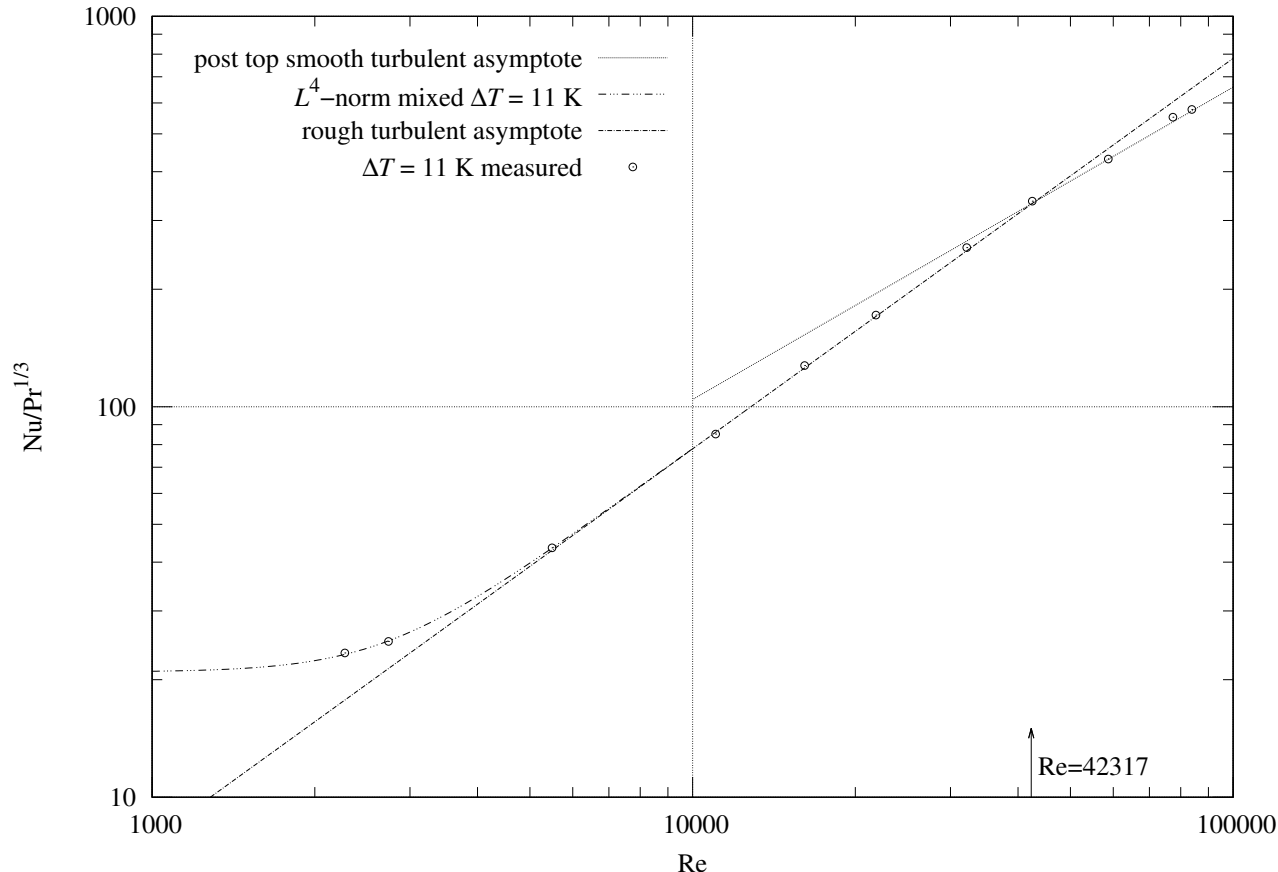


Figure 8 Convection from rough plate

⁷ Self-similarity is similarity between shapes at different scales; but these blocks are all the same size.

⁸ In Figure 8 at $\text{Re} < 5500$ the “ L^4 -norm mixed $\Delta T = 11 \text{ K}$ ” trace for equation (18) is corrected for mixed convection, as described in *Turbulent Mixed Convection from an Isothermal Plate*[8]. At $\text{Re} > 50000$ the “post top smooth turbulent asymptote” trace (having slope $4/5$) shows that convection is mostly from the smooth post tops and is no longer behaving as (slope 1) equation (18). A plate with four times the number of blocks having $1/4$ the cross-section would move the crossover to smooth turbulent convection above $\text{Re} = 200000$.

10. Sand-Roughness

Modeling sand grains as unit radius spheres glued to the plate surface in a square array and modeling the space not covered by a sphere as glue of height $0 \leq \bar{g} \leq 1$, the mean height of the enclosing square cell of area A containing a unit sphere is:

$$\bar{z} = \left(\int_0^1 2\pi x (\sqrt{1-x^2} + 1) dx + (A - \pi)\bar{g} \right) / A = \left(\frac{5}{3}\pi + (A - \pi)\bar{g} \right) / A$$

The (dimensionless for unit radius sphere) root-mean-squared height-of-roughness R_q is:

$$R_q = \frac{1}{2} \sqrt{\left(\int_0^1 2\pi x (\sqrt{1-x^2} + 1 - \bar{z})^2 dx + (A - \pi)(\bar{z} - \bar{g})^2 \right) / A}$$

For glue level $1 < \bar{g} < 2$, the grains are more than 50% submerged. Let $r_g = \sqrt{1 - (\bar{g} - 1)^2} = \sqrt{2\bar{g} - \bar{g}^2}$ be the radius of the glue opening through which the sphere is exposed. The mean height of the enclosing square cell of area A containing a unit sphere is then:

$$\bar{z} = \left(\int_0^{r_g} 2\pi x (\sqrt{1-x^2} + 1) dx + (A - \pi r_g^2)\bar{g} \right) / A = \left(\frac{4 + 3\bar{g}^2 - 2\bar{g}^3}{3} \pi + (A - \pi r_g^2)\bar{g} \right) / A$$

For this submerged case, R_q is:

$$R_q = \frac{1}{2} \sqrt{\left(\int_0^{r_g} 2\pi x (\sqrt{1-x^2} + 1 - \bar{z})^2 dx + (A - \pi r_g^2)(\bar{z} - \bar{g})^2 \right) / A}$$

Figure 9 shows the conversion factors from ε to k_S as a function of relative glue thickness.

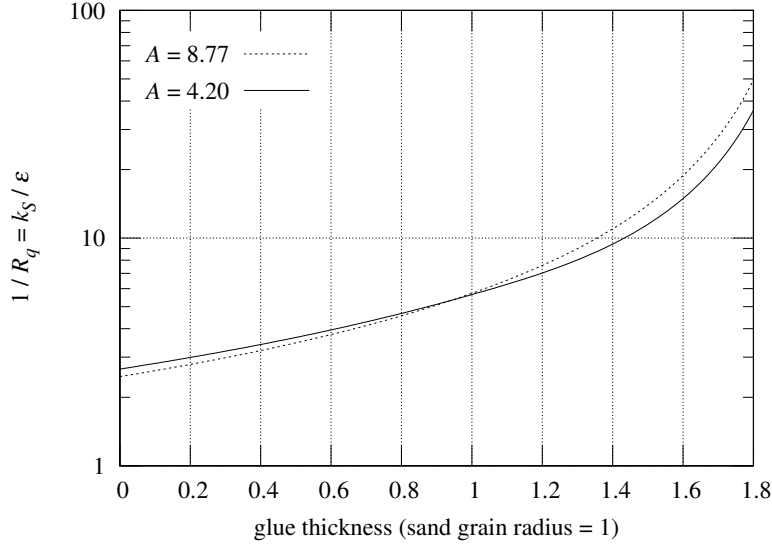


Figure 9 ε to k_S conversion factor vs. glue thickness and cell area A

Because of the sand-roughness scaling problem noted in Section 2, in order to compare the Prandtl and Schlichting[1] formula (1) with formula (16) of present work, different $k_S/\varepsilon = 1/R_q$ conversion factors must be used at large and small k_S values.

The geometric mean of the cell area A for the larger grains is $4/(0.08 \times 0.04 \times \sqrt{150 \times 590}) \approx 4.2$ (from Table 1) relative to a unit radius sphere. With $L/\varepsilon = 100$, compare c_f (for $L/k_S = R_q L/\varepsilon$) in Table 2 with $f_c = 0.0157$ calculated from formula (16):

| \bar{g} | \bar{z} | $1/R_q$ | L/k_S | c_f |
|-----------|-----------|---------|---------|--------|
| 0.00 | 1.25 | 2.66 | 37.6 | 0.0241 |
| 0.88 | 1.47 | 5.03 | 19.9 | 0.0314 |
| 1.00 | 1.50 | 5.64 | 17.7 | 0.0330 |

Table 2 RMS roughness R_q versus large-grain sand-roughness k_S

$f_c = 0.0157$ is out of the range of possible c_f values with $\bar{g} \geq 0$.

The theoretical development and the tables of measurements in Pimenta, Moffat, and Kays[3] use $C_f/2$.

In Mills and Hang[2], the tables comparing data from Pimenta, Moffat, and Kays[3] with the Prandtl-Schlichting and Mills-Hang formulas display $C_f/2$ for all three sources.

Half the c_f value from the $\bar{g} = 0.88$ row in Table 2 matches $f_c = 0.0157$; and 0.88 is a plausible level of glue (less than half of the sand grain diameter).

Regardless of the etiology of this factor of 2, the Prandtl-Schlichting and Mills-Hang formulas in Figure 10 are multiplied by 0.5 to bring them into the realm of plausibility.

The geometric mean unit cell area for the smaller grains is $4/(0.02 \times 0.01 \times \sqrt{1130 \times 4600}) \approx 8.77$. With $L/\varepsilon = 1000$, the corresponding $f_c = 0.00699$. As before, there is no glue level $\bar{g} \geq 0$ whose c_f matches f_c , but half of c_f does match f_c at $\bar{g} = 1.01$ in Table 3.

| \bar{g} | \bar{z} | $1/R_q$ | L/k_S | c_f |
|-----------|-----------|---------|---------|--------|
| 0.00 | 0.60 | 2.46 | 405.8 | 0.0108 |
| 1.01 | 1.25 | 5.80 | 172.5 | 0.0140 |
| 1.50 | 1.57 | 13.95 | 71.7 | 0.0189 |

Table 3 RMS roughness R_q versus small-grain sand-roughness k_S

Afzal, Seena, and Bushra in *Turbulent flow in a machine honed rough pipe for large Reynolds numbers: General roughness scaling laws*[9] fit 5.333 for the RMS to sand-roughness conversion factor and 6.45 for the arithmetic-mean to sand-roughness conversion factor. The geometric mean of the $1/R_q$ values 5.03 and 5.80 (≈ 5.40) is within 2% of 5.333 and not close to 6.45. This supports the RMS height-of-roughness being the true metric for surface roughness.

In *Skin-friction behavior in the transitionally-rough regime*[10], Flack, Schultz, Barros, and Kim measure skin-friction from grit-blasted surfaces in a duct. They write “The root-mean-square roughness height (k_{rms}) is shown to be most strongly correlated with the equivalent sand-roughness height (k_S) for the grit-blasted surfaces.”

5.33 (from Afzal, Seena, and Bushra) is used as the RMS to sand-roughness conversion factor for the Mills-Hang formula in Figure 10.

Figure 10 shows that the corrected⁹ Mills-Hang formula (2) is nearly coincident with equation (16) over the range $100 < L/\varepsilon < 1000$; so it is an improvement compared to Prandtl and Schlichting’s formula (1). This close match in the completely rough regime supports the present theory with the measurements from Pimenta, Moffat, and Kays[3] modeled by Mills and Hang[2].

At $L/\varepsilon > 1000$, the inset graph in Figure 10 shows that both Mills-Hang and Prandtl-Schlichting suffer from the scale error discussed in Section 2, growing to -13% and -18% relative to equation (16) at $L/\varepsilon = 10^6$.

⁹ See footnote about the Mills-Hang formula in Section 2.

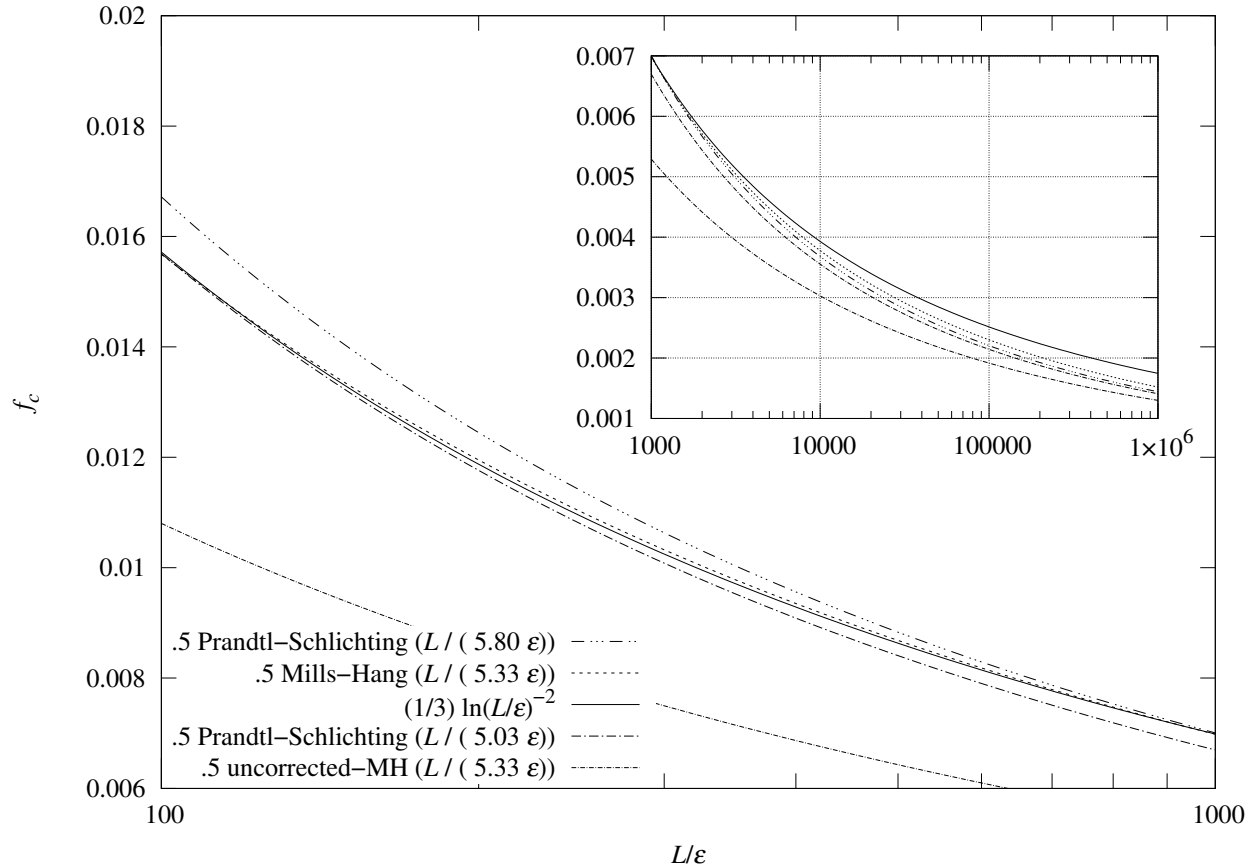


Figure 10 Fully rough (turbulent) friction coefficient

11. Transitional Rough Regime

Afzal, Seena, and Bushra[9] (also Schlichting[4]) relate that the turbulent flow inside commercial pipes behaves differently from the flow inside Nikuradse’s sand coated pipes in the transitional rough regime. While the skin-friction coefficients for commercial pipes are monotonically decreasing with increasing Re on the Moody diagram, the diagram for Nikuradse’s pipes have a local minimum just to the right of the smooth skin-friction line, which they term “inflectional”.

The Prandtl-Schlichting plate model apparently inherited the inflectional curve from Nikuradse’s pipes. The total coefficient of resistance (c_f) Moody diagram from Prandtl and Schlichting[1] shows a 10% dip spread over a decade of Re just to the right of the smooth skin-friction line before leveling out towards the right.

Prandtl and Schlichting[1] put the boundary between the transitional rough and fully rough regimes for a plate at roughness Reynolds number $Re_k = Re k_s / L = 70.8$. Pimenta, Moffat, and Kays[3] put it at 65.

Pimenta, Moffat, and Kays[3] write that, while the agreement of their data with the Prandtl-Schlichting plate model is “rather good” in the fully rough regime, their apparatus does not have the same behavior as “Nikuradse’s sand-grain pipe flows in the transition region”.

Figure 11 shows the local skin-friction coefficient versus x/k_S for the Pimenta, Moffat, and Kays sphere-roughened plate at three speeds of flow. The averages of these local coefficients (from $800 < x/k_S < 2800$) are 0.00241, 0.00240, and 0.00233. These values are within 3.5% of each other, less than the 10% spread predicted by Prandtl and Schlichting[1].

For a self-similar roughness (producing turbulence) there should be no variation in skin-friction coefficient with Reynolds number. The less than 3.5% spread in average friction coefficients supports the new theory more strongly than it supports the Prandtl and Schlichting plate theory.

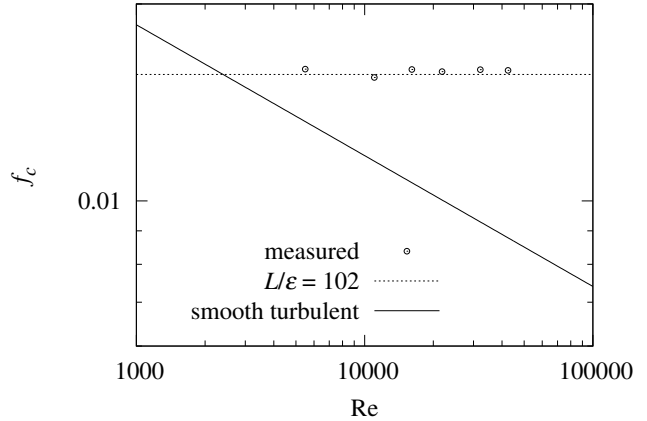
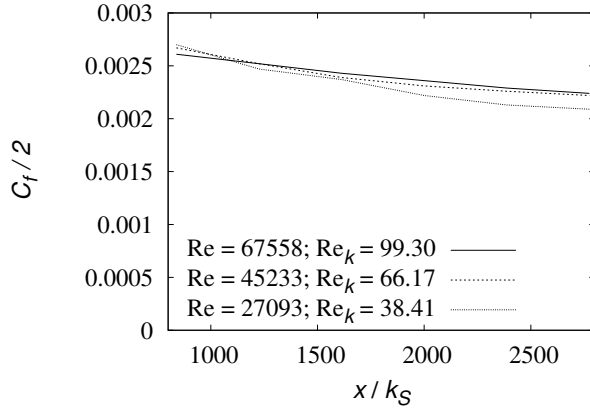


Figure 11 Local C_f for sphere-roughened plate **Figure 12** f_c vs. Re for bi-level plate

For the 3 mm roughness bi-level plate:¹⁰

$$Re = Re_k \frac{L}{k_s} = Re_k \frac{L}{\epsilon R_q} = 70.8 \frac{.305}{.003/5.33} \approx 38365$$

So Figure 12 covers most of the transitionally rough regime and some of the fully rough regime.

Figure 12 is a Moody diagram of the 3 mm RMS roughness bi-level plate measurements converted to friction coefficients f_c using the Chilton and Colburn J-factor analogy (17). The “measured” points hew closely to the “ $L/\epsilon = 102$ ” line at $f_c = 0.0156$ and are level within their expected measurement uncertainties.¹¹

This self-dissimilar surface having negligible dependence on Re is evidence that formula (16) applies over the range of turbulent flow from isotropic rough plates.

This independence from Re contrasts with rough pipe interiors and Prandtl and Schlichting’s[1] plate theory, in which f_c depends on Re except in the completely rough regime.

12. Roughness in Pipes

Self-similar roughness is not applicable to pipe interiors because, while the self-similar plate height-of-roughness grows proportionally to length in the direction of flow, the characteristic-length diameter is fixed in cylindrical pipes. Looking at roughness more generally may provide some insights.

The skin-friction coefficient of plate roughness being independent of Re is evidence that the monotonic/inflectional variation in pipe skin-friction coefficient with Re is not due to some property of isotropic roughness. Commercial pipe interiors may well have longitudinal roughness different from circumferential roughness as a result of their manufacturing processes, for example extrusion.

Assuming Nikuradse’s sand-roughness samples had isotropic roughness, why aren’t their Moody diagram traces level?

The characteristic-length for pipe interiors is the diameter of the pipe; but the bulk flow is longitudinal. It is not clear that the longitudinal roughness should be measured against the same characteristic-length as the circumferential roughness. If the characteristic-lengths should be different, then pipe skin-friction coefficient should be formulated as a function of the circumferential and longitudinal roughness profiles (and Re) instead of a single surface roughness (and Re).

¹⁰ The sand-roughness to RMS height-of-roughness conversion factor $1/R_q = 5.33$ is discussed in Section 10.

¹¹ Convection at $Re < 5500$ is mixed with natural convection for which the analogy doesn’t apply; those measurements aren’t shown in Figure 12.

13. Conclusions

- For a flat surface with isotropic RMS height-of-roughness $\varepsilon > 0$ which is producing rough turbulence in a steady flow of strength Re , the skin-friction coefficient and total forced convection formulas are:

$$f_c = \frac{1}{3 \ln^2(L/\varepsilon)} \quad Nu = \frac{Re Pr^{1/3}}{6 \ln^2(L/\varepsilon)} \quad \frac{L}{\varepsilon} \gg 1$$

- These formulas hold for both transitional rough and fully rough flow regimes.
- These formulas are supported by measurements of self-dissimilar plates by the author and by Pimenta, Moffat, and Kays in both the transitional rough and fully rough regimes.

Acknowledgments

The idea of self-similar roughness grew out of a discussion with Nina Koch about turbulence self-similarity. Thanks to John Cox for machining the bi-level plate.

14. Nomenclature

| | |
|--------|--|
| | Nu = average Nusselt number (convection) |
| | Pr = fluid Prandtl number |
| | Re = Reynolds number of flow parallel to the plate |
| Re_k | $= Re k_S/L$ = roughness Reynolds number |
| | A = area of square cell containing sphere sand grain (m ²) |
| | C_D = Mills and Hang total friction coefficient |
| | $C_f/2$ = Pimenta, Moffat, and Kays local friction coefficient |
| | c_f = Prandtl and Schlichting total friction coefficient |
| | f_c = total friction coefficient |
| | \bar{g} = height of glue (m) |
| | $G(x, w)$ = Gray-code profile function |
| j | $= \log_2 w$ = positive integer |
| | k_S = sand-roughness (m) |
| | L = plate characteristic-length (m) |
| | n = branching factor of profile roughness function |
| | R_q = dimensionless RMS height-of-roughness |
| | r_g = radius of glue opening exposing unit sphere |
| | u = fluid velocity (m/s) |
| | u_R = vertical roughness fluid velocity (m/s) |
| | $w = 2^j$ = integer power of two |
| | $W(x, w)$ = wiggliest integer self-similar profile function |
| | $Y(x, w)$ = integer self-similar profile function |
| | x, y = distance (m) |
| | $z(x)$ = profile roughness function (m) |
| | $z(x, y)$ = surface roughness function (m) |
| | \bar{z} = mean height of roughness (m) |
| | Z = profile roughness function random variable (m) |

Greek Symbols

| | |
|---------------|--|
| ϵ | = RMS profile height-of-roughness (m) |
| ε | = RMS surface height-of-roughness (m) |
| ρ | = fluid density (kg/m ³) |
| τ | = fluid shear stress (N/m ²) |

15. References

- [1] L. Prandtl and H. Schlichting. *The Resistance Law for Rough Plates*. Translation (David W. Taylor Model Basin). Navy Department, the David W. Taylor Model Basin, 1934. Translated 1955 by P.S. Granville.
- [2] A. F. Mills and Xu Hang. On the skin friction coefficient for a fully rough flat plate. *J. Fluids Eng*, 105(3):364–365, 1983.
- [3] M. M. Pimenta, R. J. Moffat, and W. M. Kays. *The Turbulent Boundary Layer: An Experimental Study of the Transport of Momentum and Heat with the Effect of Roughness*. Department of Mechanical Engineering, Stanford University, 1975.
- [4] Hermann Schlichting, Klaus Gersten, Egon Collaborateur. Krause, Herbert Collaborateur. Oertel, and Katherine Mayes. *Boundary-layer theory*. Springer, Berlin, Heidelberg, Paris, 2000. Corrected printing 2003.
- [5] Frank White. *Viscous Fluid Flow, 3rd Edition*. McGraw-Hill, 2006.
- [6] Mitchell G. Newberry and Van M. Savage. Self-similar processes follow a power law in discrete logarithmic space. *Phys. Rev. Lett.*, 122:158303, Apr 2019.
- [7] A. Jaffer. Convection measurement apparatus and methodology, 2019. [Online; accessed 20-June-2019].
- [8] A. Jaffer. Turbulent mixed convection from an isothermal plate, 2019. [Online; accessed 13-June-2019].
- [9] Noor Afzal, Abu Seena, and A. Bushra. Turbulent flow in a machine honed rough pipe for large reynolds numbers: General roughness scaling laws. *Journal of Hydro-environment Research*, 7(1):81–90, 2013.
- [10] Karen A Flack, Michael P Schultz, Julio M Barros, and Yechan C Kim. Skin-friction behavior in the transitionally-rough regime. *International Journal of Heat and Fluid Flow*, 61:21–30, 2016.